Non-Hermitian Thouless pumping: Interplay between topological charge pumping and directional tunneling

Xiaoyi Yang [1,*] Chengming Tan [2,*] Yangqian Yan [3,†] and Ren Zhang [1,4,‡]
[1] *MOE Key Laboratory for Nonequilibrium Synthesis and Modulation of Condensed Matter, Shaanxi Province Key Laboratory of Quantum Information and Quantum Optoelectronic Devices, School of Physics, Xi'an Jiaotong University, Xi'an 710049, China*
[2] *Hefei National Research Center for Physical Sciences at the Microscale and School of Physical Sciences, University of Science and Technology of China, Hefei 230026, China*
[3] *Department of Physics, The Chinese University of Hong Kong, Hong Kong SAR, China*
[4] *Hefei National Laboratory, Hefei 230088, China*

(Received 21 April 2024; revised 26 April 2025; accepted 30 April 2025; published 14 May 2025)

Motivated by experimental realizations of the lattice models with directional tunneling and the generalized bulk-edge correspondence brought by a similarity transformation, we study the topological charge pumping using the Rice-Mele (RM) model with directional tunneling (also termed as the non-Hermitian RM model). In momentum space, through a similaritylike transformation, we map the non-Hermitian RM model to a Hermitian one. Under the biorthogonal basis, the pumping is dictated by a Chern number of the Hermitian RM model. This can be verified by experiments where both the non-Hermitian RM model and its Hermitian conjugation are realized. Under the right-right vector basis, which is relevant to experiments where only the non-Hermitian one is required, we find that the charge pumping contains a dynamical and a topological part. To reveal the topological contribution, an experimental scheme of canceling the dynamical term is proposed.

DOI: 10.1103/PhysRevA.111.053308

I. INTRODUCTION

Topological Thouless pumping has been both predicted and observed across a range of experimental settings involving fermions and bosons, including ultracold atoms [1–3] and photonics [4–6]. The charge pumped in a cycle is quantized and characterized by a Chern number [7–13]. The Rice-Mele (RM) model, a paradigm to study Thouless pumping [14–25], has been implemented in a variety of systems, including cold atoms [16,26,27], optics [28–31], and superconducting circuits [32].

Owing to theoretical and experimental advances in non-Hermitian physics [33–63], non-Hermitian charge pumping has been extensively explored [64–70]. Many unexpected transport effects have been unraveled in non-Hermitian systems, such as spontaneous topological pumping and fast Thouless pumping [68,69,71]. Despite these advancements, several fundamental questions remain open. For instance, how do the topological charge pumping and directional tunneling interplay? What is the difference between wave-packet displacements in a non-Hermitian system, where one has to distinguish between the left and right vectors? Furthermore, how can the topological contribution be effectively isolated from the total displacement in experimental measurements?

To answer these questions, in this paper, we use the non-Hermitian RM model [illustrated in Fig. 1(a)] to study the interplay between the topological charge pumping and directional tunneling. Our main conclusions are summarized as follows. (1) We first show that, in momentum space, the non-Hermitian and Hermitian RM models are connected by a class of *similaritylike* transformation, which contrasts to the similarity transformation in real space. This similarity-like transformation unravels the relation between the Chern numbers of the Hermitian and non-Hermitian RM models. (2) Under the biorthogonal basis, the topological charge pumping of the non-Hermitian RM model follows the Chern number of the Hermitian bulk Hamiltonian, which is proved by the similarity transformation. (3) Under the right-right vector basis, we show that the displacement is contributed by both a dynamical and a topological part, and we provide a method to extract the topological part from the total displacement. Importantly, the topological part follows the Chern number of the non-Hermitian RM model. In Fig. 1(b), we schematically illustrate the charge pumping when the initial state is localized in the lower (blue arrow) and upper (red arrow) band, respectively.

II. MODEL

We consider the RM model with directional intracell hopping strength as shown in Fig. 1(a), and write the Hamiltonian as [72,73]

$$\hat{H}(t) = \sum_n^N \left[\left(J_1(t) + \frac{\gamma}{2} \right) a_n^\dagger b_n + \left(J_1(t) - \frac{\gamma}{2} \right) b_n^\dagger a_n \right] + J_2 \sum_n^N (a_{n+1}^\dagger b_n + \text{H.c.}) + \Delta(t) \sum_n^N (a_n^\dagger a_n - b_n^\dagger b_n), \tag{1}$$

*These authors contributed equally to this work.
†Contact author: yqyan@cuhk.edu.hk
‡Contact author: renzhang@xjtu.edu.cn

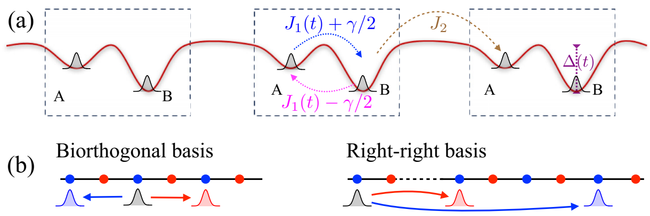

FIG. 1. (a) Schematics of the Rice-Mele model with directional tunneling. The dotted box indicates a unit cell composed of sublattices A and B. (b) Illustration of the wave-packet displacement in a cycle under biorthogonal and right-right basis. Blue and red solid circles denote sublattices A and B, respectively. The gray wave packet represents the initial state. Blue and red wave packets represent the final state when the initial state is localized in the lower and upper band.

where $J_1(t) \pm \gamma/2$ and J_2 denote the time-dependent intra- and intercell hopping strength, respectively; γ is the strength imbalance of the directional tunneling. $\Delta(t)$ is the time-dependent staggered on-site potential. $a_n^\dagger$ and $b_n^\dagger$ (a_n and b_n) are creation (annihilation) operators on sublattices A and B of unit cell n, respectively. When γ is zero, Eq. (1) reduces to the Hermitian RM model, for which the topological charge pumping is governed by the Chern number [14–25].

To achieve topological charge pumping, the Hamiltonian should be periodic in the parameter space. In this work, we consider the following case: $J_1(t) = J_0 + E_0 \cos(\omega t)$, $J_2 = E_0$, and $\Delta(t) = E_0 \sin(\omega t)$, where J_0 is the average intracell hopping value and ω is the modulation frequency; here, J_0, E_0 are the characteristic energies. To meet the condition of adiabaticity, we require $\omega \ll J_0, E_0$. Nevertheless, ω can be comparable to or even larger than γ.

III. SIMILARITYLIKE TRANSFORMATION

Under periodic boundary conditions, we write the bare non-Hermitian Rice-Mele in momentum space as

$$\hat{H}(k,t) = d_x\hat{\sigma}_x + \left(d_y + i\frac{\gamma}{2}\right)\hat{\sigma}_y + d_z\hat{\sigma}_z, \tag{2}$$

where $d_x = J_1(t) + J_2\cos(k)$, $d_y = J_2\sin(k)$, $d_z = \Delta(t)$, and $\hat{\sigma}_{x,y,z}$ denote the Pauli matrices. Throughout this work, we set the lattice constant to unity. In real space with open boundary conditions (OBCs), the non-Hermitian Hamiltonian in Eq. (1) maps to a Hermitian one by a similarity transformation [74]. However, in general, such a mapping cannot be established in momentum space. As one of the central results of this work, we find that the non-Hermitian Hamiltonian in Eq. (2) nevertheless maps to a Hermitian one by a *similaritylike* transformation

$$\alpha(k)\hat{T}^{-1}\hat{H}(k,t)\hat{T} = \hat{\mathcal{H}}(k,t). \tag{3}$$

By similaritylike, we mean that besides the similarity transformation $\hat{T}$, there is an extra factor $\alpha(k)$ that is either complex or real [see Appendix A for the explicit expression of $\alpha(k)$ and $\hat{T}$].

We would like to make two comments before further proceeding: (1) $\hat{H}(k,t)$ in Eq. (3) is obtained by Fourier transforming the non-Hermitian Hamiltonian in Eq. (1), while

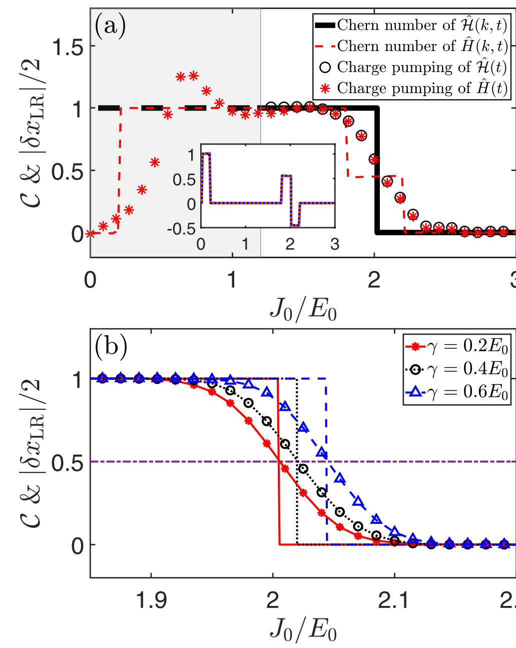

FIG. 2. (a) The Chern number of the non-Hermitian Rice-Mele model, and the charge pumping in a cycle with $\gamma = 0.4E_0$ and $\omega = 0.3E_0$. The dashed black line is the analytical continuation of the solid black line. Inset: The blue dashed and purple solid lines denote the integral of $\Omega^T_{tk}(k,t) - \Omega^T_{kt}(k,t)$ and difference of the Chern numbers of the Hermitian and non-Hermitian Hamiltonians, respectively. (b) The Chern number (lines) and the displacement (symbols) defined under the biorthogonal basis as a function of J_0. Here, $\omega = 0.01E_0$. The horizontal dashed-dotted line is a guide for the eye.

$\hat{\mathcal{H}}(k,t)$ denotes the Fourier transformation of the corresponding Hermitian Hamiltonian $\hat{\mathcal{H}}(t)$ in real space. These two real-space Hamiltonians are linked by a similarity transformation [74]. (2) The similaritylike transformation applies to the case where the energy spectrum is either real or complex, whereas the similarity transform only applies to the real energy spectrum. If the spectrum is real, the similaritylike transformation reduces to the similarity transformation, i.e., $\alpha(k) = 1$. One of the applications of the similaritylike transformation is that it connects the topological numbers of the bare non-Hermitian Hamiltonian $\hat{H}(k,t)$ and the transformed Hermitian one $\hat{\mathcal{H}}(k,t)$. In general, we define the Chern number as

$$\mathcal{C} = \frac{1}{2\pi}\int_0^{2\pi/\omega} dt \int_{-\pi}^{\pi} dk\,\Omega(k,t), \tag{4}$$

where Ω denotes the Berry curvature.

First, for non-Hermitian RM model, the Berry curvature under the biorthogonal basis is defined as

$$\Omega(k,t) = i_{\rm L}\langle \partial_t u(k,t)|\partial_k u(k,t)\rangle_{\rm R} - i_{\rm L}\langle \partial_k u(k,t)|\partial_t u(k,t)\rangle_{\rm R}; \tag{5}$$

here, $|u(k)\rangle_{\rm R}$ and $|u(k)\rangle_{\rm L}$ are the eigenstates of $\hat{H}(k,t)$ and $\hat{H}^\dagger(k,t)$, respectively. Based on this definition, we obtain the Chern number [red dashed line in Fig. 2(a)]. It has been pointed out that the Chern number is not quantized near

$J_0 \sim 2E_0$ and the topological transition indicated by $\mathcal{C}$ also does not follow the bulk-edge correspondence [75].

Second, by the similaritylike transformation in Eq. (3), we obtain the Hamiltonian of the RM model (see Appendix A),

$$\hat{\mathcal{H}}(k,t) = \begin{pmatrix} \Delta(t) & \sqrt{J_1^2(t) - \frac{\gamma^2}{4}} + J_2 e^{-ik} \\ \sqrt{J_1^2(t) - \frac{\gamma^2}{4}} + J_2 e^{ik} & -\Delta(t) \end{pmatrix}. \tag{6}$$

The corresponding Berry curvature is defined by

$$\tilde{\Omega}(k,t) = i\langle \partial_t \tilde{u}(k,t)|\partial_k \tilde{u}(k,t)\rangle - i\langle \partial_k \tilde{u}(k,t)|\partial_t \tilde{u}(k,t)\rangle, \tag{7}$$

where $|\tilde{u}(k,t)\rangle$ is the eigenstate of $\hat{\mathcal{H}}(k,t)$. The corresponding Chern number is showcased by the black solid line in Fig. 2(a). Note that the similarity transformation is inapplicable in the interval $J_0 \leqslant E_0 + \gamma/2$, and the Chern number is not well defined. Therefore, the Chern number in this interval is an extension of the well-defined Chern number (black solid line), as shown by the black dashed line in Fig. 2(a). It is clear that the Chern number becomes quantized, and the bulk-edge correspondence is restored [75].

Because the two momentum-space Hamiltonians are connected via similaritylike transformations, we expect that the Chern numbers are related to each other. To see this, we write the relation between the eigenstates of $\hat{H}(k,t)$ and $\hat{\mathcal{H}}(k,t)$ as $|\tilde{u}(k,t)\rangle = \hat{T}^{-1}|u(k,t)\rangle_R$ and $\langle \tilde{u}(k,t)| = {}_L\langle u(k,t)|\hat{T}$. Upon substituting this relation into Eq. (7), we find the relation between $\Omega(k,t)$ and $\tilde{\Omega}(k,t)$,

$$\tilde{\Omega}(k,t) = \Omega(k,t) + \left[\Omega^T_{tk}(k,t) - \Omega^T_{kt}(k,t)\right], \tag{8}$$

where $\Omega^T_{tk}(k,t)$ originates from the similaritylike transformation, and reads

$$\begin{aligned} \Omega^T_{tk}(k,t) &= i_L\langle \partial_t u(k,t)|\hat{T}(\partial_k \hat{T}^{-1})|u(k,t)\rangle_R \\ &\quad + i_L\langle u(k,t)|(\partial_t \hat{T})(\partial_k \hat{T}^{-1})|u(k,t)\rangle_R \\ &\quad + i_L\langle u(k,t)|(\partial_t \hat{T})\hat{T}^{-1}|\partial_k u(k,t)\rangle_R. \end{aligned} \tag{9}$$

Using this extra "Berry curvature," we obtain a corresponding topological number defined in Eq. (4). According to Eq. (8), the difference of the Chern numbers of $\hat{\mathcal{H}}(k,t)$ and $\hat{H}(k,t)$ is determined by this extra Berry curvature, as illustrated in Fig. 2. Here, the red dashed and black solid lines denote the Chern numbers of $\hat{H}(k,t)$ and $\tilde{H}(k,t)$, respectively, and the difference of them is shown by the blue dotted line in the inset, which equals the integral of the second term in Eq. (8) (the solid purple line).

IV. CHARGE PUMPING UNDER BIORTHOGONAL BASIS

In order to investigate the physical consequence of topology, we study the charge pumping, i.e., the center-of-mass displacement of a wave packet in a cycle. To observe quantized pumping, we need to evenly occupy the energy band, which could be achieved by choosing the Wannier state as the initial state. For the non-Hermitian RM model in Eq. (1), the right Wannier state centered at the jth unit cell reads

$$|w_j\rangle_R = \frac{1}{N}\sum_{k=\delta_k}^{N\delta_k}\sum_{m=1}^{N} e^{i(m-j)k}\,|m\rangle \otimes |u(k)\rangle_R, \tag{10}$$

where $\delta_k = 2\pi/N$ and $|u(k)\rangle_R$ is the right eigenstate of $\hat{H}(k,t)$. The left Wannier state $|w_j\rangle_L$ is similarly defined using $|u(k)\rangle_L$. With the left and right Wannier states, we have two options for defining the displacement. First, using the biorthogonal basis, we define the position of the Wannier center as

$$x_{LR}(t) = {}_L\langle w_j|\hat{U}^{-1}(t)\hat{x}\hat{U}(t)|w_j\rangle_R, \tag{11}$$

where $\hat{U}(t) = \mathcal{T}e^{-i\int_0^t \hat{H}(\tau)d\tau}$ is the evolution operator with $\mathcal{T}$ denoting time order.

After a cycle, the displacement of the Wannier center is $\delta x_{LR} = x_{LR}(T) - x_{LR}(0)$. Figure 2 shows the displacement (red stars) driven by the non-Hermitian Hamiltonian $\hat{H}$ with $\gamma = 0.4E_0$. We emphasize that the quantized displacements were obtained only in the interval $J_0 > E_0 + \gamma/2$. When $J_0 \leqslant E_0 + \gamma/2$, the energy spectrum under OBC becomes complex (see Appendix B), indicating the presence of exceptional points (EPs). In an evolution cycle, the system passes through the EPs, namely $J_0 + E_0\cos(\omega t) = \pm\gamma/2$, four times. When EPs appear (denoted by the gray area in Fig. 2), the quantized charge pumping disappears, even though the Chern number might still appear to be quantized.

Note that the evolution operator of the non-Hermitian model maps to that of the Hermitian one by a similarity transformation as $\hat{U}(t) = S(t)\tilde{U}(t)S^{-1}(0)$, where $\tilde{U}(t) = \mathcal{T}e^{-i\int_0^t \hat{\mathcal{H}}(\tau)d\tau}$ and $\hat{S}$ is the similarity-transformation matrix [74]. Thus, we rewrite the time-dependent Wannier center position as

$$x_{LR}(t) = {}_L\langle w_j|S(0)\tilde{U}^{-1}(t)\hat{x}\tilde{U}(t)S^{-1}(0)|w_j\rangle_R. \tag{12}$$

Then, we interpret $x_{LR}(t)$ as the position expectation value under $S^{-1}(0)|w_j\rangle_R$ and ${}_L\langle w_j|S(0)$. Our results show that it is approximately identical to the displacement of the Wannier center under the driving of the corresponding Hermitian Hamiltonian,

$$\tilde{x}(t) = \langle \tilde{w}_j|\tilde{U}^{-1}(t)\hat{x}\tilde{U}(t)|\tilde{w}_j\rangle, \tag{13}$$

where $|\tilde{w}_j\rangle$ is the Wannier state of $\hat{\mathcal{H}}(t)$. By comparing Eqs. (12) and (13), we conclude that $|\tilde{w}_j\rangle \approx S^{-1}|w_j(m)\rangle_R$, which was numerically verified (see Appendix C). Figure 2(a) shows the displacement in a cycle. The red stars depict the displacement driven by the non-Hermitian Hamiltonian $\hat{H}(t)$, while the black circles are for the displacement driven by the Hermitian Hamiltonian $\hat{S}^{-1}\hat{H}(t)\hat{S}$. These two curves are nearly identical when $J_1(t) > E_0 + \gamma/2$. This alignment implies that both scenarios follow the same Chern number (black line) of the Hermitian Hamiltonian.

Figure 2(b) shows the displacement in a cycle (lines with symbols) and the Chern number (lines) for different γ with $\omega = 0.01E_0$. We observe that the topological phase transition happens at $J_0 = E_0 + \sqrt{J_2^2 + \gamma^2/4}$, indicated by the sudden change of the Chern number. Because of the nonadiabatic nature of the charge pumping, the displacement is a smooth function. At the phase transition point, the energy bands close, breaking adiabaticity. However, adiabaticity is restored away from this point as the energy gap reopens. Notably, the energy gap varies symmetrically around the transition point. This phenomenon leads to a symmetric deviation of the displacement on both sides. Nevertheless, we find that the transition

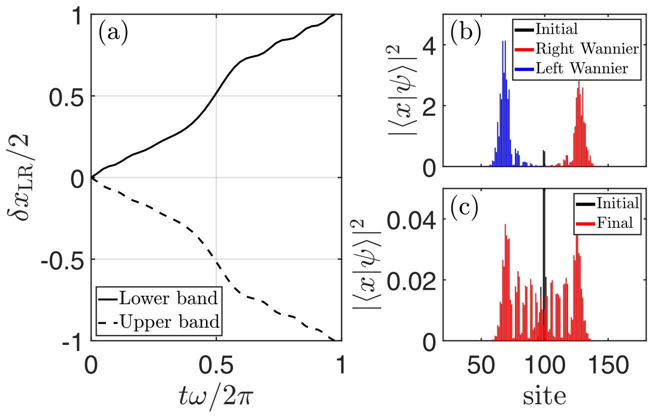

FIG. 3. (a) The displacement of the Wannier center in a cycle. The solid and dashed lines are for the initial state localized in the lower and upper bands, respectively. (b) The wave packet of the lower band driven by the non-Hermitian Hamiltonian after a cycle. The red (right half) and blue (left half) histograms are evolved from the initial wave packet of the right and left vectors, respectively. (c) The wave packet of the lower band driven by the Hermitian Hamiltonian. The black (central peak) and the red histogram are for the initial- and final-state wave packets, respectively. Here, $\gamma = 0.4E_0$, $J_0 = 1.5E_0$, and $\omega = 0.3E_0$.

points locate exactly at the displacement $x_{\rm LR} = 0.5$, which suggests that $\delta x_{\rm LR}(T)$ follows the Chern number of the Hermitian Hamiltonian.

To measure the charge pumping, we require two experiments, in which the Hamiltonians are Hermitian conjugates to each other [76,77]. Figure 3 shows the evolution of the wave packet and the displacement of the Wannier center over time. In Fig. 3(a), the solid (dashed) line corresponds to an initial state which is localized in the lower (upper) band. These two states have opposite directional topological charge pumping. We choose $\gamma = 0.4E_0$, $t_0 = 1.5E_0$, and $\omega = 0.3E_0$, and consider a chain of 100 unit cells. The initial state locates at the center, as depicted by the black histogram in Fig. 3(b). The left and right Wannier states are driven by $\hat{H}^\dagger(t)$ and $\hat{H}(t)$, respectively, resulting in blue and red wave packets after a cycle. The wave packet driven by the Hermitian Hamiltonian $\hat{S}^{-1}\hat{H}(t)\hat{S}$ is shown in Fig. 3(c). Although Figs. 3(b) and 3(c) showcase two distinct final wave packets, the displacements in a cycle are identical.

V. CHARGE PUMPING UNDER RIGHT-RIGHT BASIS

We now define the charge pumping displacement using the right-right vector basis, which can be directly obtained in a single experimental measurement. In this case, the expectation value of the Wannier center position is given by

$$x_{\rm RR}(t) = {}_{\rm R}\langle w_j|\hat{U}^\dagger(t)\hat{x}\hat{U}(t)|w_j\rangle_{\rm R}, \tag{14}$$

where $\hat{U}(t)$ denotes the time-evolution operator and $|w_j\rangle_{\rm R}$ is the initial Wannier state in the right vector basis. Figure 4 illustrates the characteristics of charge pumping defined in the right-right vector. As shown in Figs. 4(a) and 4(b), the wave packet exhibits directional motion, regardless of whether the initial state lies in the upper or lower band. This indicates the

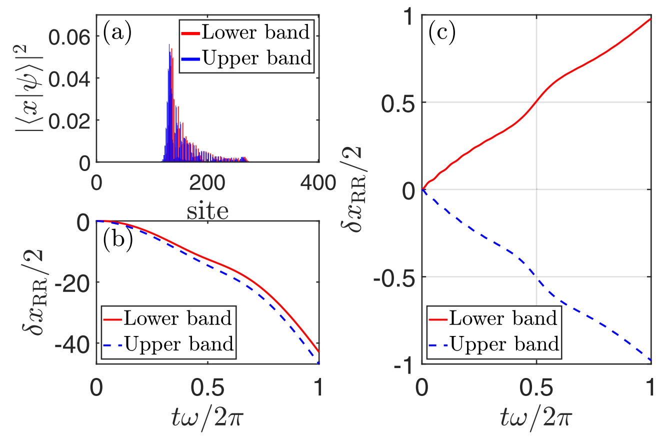

FIG. 4. The charge pumping defined under right-right vectors. (a) The final Wannier wave packet after a cycle. (b) The total displacement as a function of time. (c) The topological part of the displacement extracted from the total displacement. Here, $\gamma = 0.04E_0$, $J_0 = 1E_0$, and $\omega = 0.1E_0$.

displacement of the Wannier center contains both dynamical and topological contributions. A natural question then arises: How can one isolate the topological component from the total displacement? The key observation is that the dynamical contributions for the upper and lower bands are identical, while the topological components are equal in magnitude but opposite in sign. Therefore, the average displacement of the two bands reflects the dynamical part, whereas subtracting this average from the displacement of each band yields the topological contribution. As shown in Fig. 4(c), the extracted topological displacement is quantized over one pumping cycle. A similar method has been adopted in the investigation of the momentum distribution in spin-orbit coupled quantum gases [78,79].

To establish the correspondence between displacement and the Chern number, we compute the Chern number under the right-right vector basis by replacing ${}_{\rm L}\langle u(k,t)|$ with ${}_{\rm R}\langle u(k,t)|$ in Eq. (5). In contrast to the biorthogonal basis, a well-defined physical Chern number does not exist in the intervals $J_0 \in [-E_0 + J_2 - \gamma/2, -E_0 + J_2 + \gamma/2]$ and $J_0 \in [E_0 + J_2 - \gamma/2, E_0 + J_2 + \gamma/2]$. This behavior is consistent with the fact that, outside these intervals, the energy of the states at $k = 0$ and $k = \pi$ remains real even under periodic boundary conditions (PBCs), whereas within these intervals the energy becomes complex. The emergence of complex energy indicates the presence of exceptional points (EPs) in the PBC spectrum, and such EPs destroy the quantization of the Chern number. As the non-Hermiticity parameter γ increases, the range supporting quantized topological charge pumping becomes narrower, consistent with the shrinking region of the well-defined Chern number. These results confirm that the topological charge pumping under the right-right vector basis follows the Chern number of the non-Hermitian Hamiltonian (see Appendix C for details).

VI. CONCLUSIONS AND OUTLOOK

We studied the interplay between topological charge pumping and directional tunneling. Using the RM model, we showed that in momentum space, the non-Hermitian and Hermitian models are connected via a similaritylike transformation. Under the biorthogonal basis, the charge pumping of the non-Hermitian RM model follows the Chern number of the corresponding Hermitian bulk Hamiltonian. Under the right-right vector basis, we demonstrated that the charge pumping consists of both dynamical and topological components, with the latter determined by the Chern number of the non-Hermitian Hamiltonian. Our results are applicable to various experimental platforms. We believe that, based on our approach, topological charge pumping under both the biorthogonal and right-right bases can be measured in future experiments. Furthermore, we find that charge pumping in the biorthogonal basis exhibits a pronounced sensitivity to the OBC spectrum, and that the presence of exceptional points (EPs) in specific states of the PBC spectrum leads to a breakdown of the quantized Chern number. These intriguing effects necessitate further in-depth investigations.

ACKNOWLEDGMENTS

We would like to thank Wei Yi and Qi Zhou for their helpful discussions, and Zhigang Wu for proofreading our manuscript. This work is supported by NSFC (Grant No. 12174300), Innovation Program for Quantum Science and Technology (Grant No.2021ZD0302001), and the Fundamental Research Funds for the Central Universities (Grant No. 71211819000001). Y.Y. acknowledges support by the Hong Kong RGC Early Career Scheme (Grant No. 24308323) and Collaborative Research Fund (Grant No. C4050-23GF), NSFC (Grant No. 12204395), and CUHK Direct Grant No. 4053676. R.Z. additionally acknowledges support from a Tang Scholar.

APPENDIX A: SIMILARITYLIKE TRANSFORMATION

In this Appendix, we use the non-Hermitian Rice-Mele (RM) model to demonstrate the similaritylike transformation. Under the periodic boundary condition, the non-Hermitian RM model in momentum space is obtained by the Fourier transformation of Eq. (1),

$$\hat{H}(k,t)=\begin{pmatrix}\Delta(t) & J_1(t)+\frac{\gamma}{2}+J_2e^{-ik}\\ J_1(t)-\frac{\gamma}{2}+J_2e^{ik} & -\Delta(t)\end{pmatrix}, \quad \text{(A1)}$$

where $J_1(t)\pm\gamma/2$ and J_2 denote the time-dependent intra- and intercell hopping strengths, respectively; $\Delta(t)$ is the time-dependent staggered on-site potential. We propose that the Hermitian and non-Hermitian Hamiltonian can be linked in momentum space using a similaritylike transformation

$$\alpha(k)\hat{T}^{-1}\hat{H}(k,t)\hat{T}=\hat{\mathcal{H}}(k,t). \quad \text{(A2)}$$

For the non-Hermitian RM model, the explicit expression of the transformation matrix $\hat{T}$ is

$$\hat{T}=\begin{pmatrix}1 & b\\ c & d\end{pmatrix}, \quad \text{(A3)}$$

where the matrix element reads and (A5)

$$\begin{aligned} b&=-\frac{\Delta(t)}{\sqrt{\left[J_1(t)-\frac{\gamma}{2}\right]\left[J_1(t)+\frac{\gamma}{2}\right]}+J_2e^{ik}},\\ c&=-\frac{\Delta(t)}{J_1(t)+\frac{\gamma}{2}+J_2e^{-ik}}, \end{aligned} \quad \text{(A4)}$$

and

$$d=\frac{4\Delta^2(t)+d_1\sqrt{4J_1^2(t)+4J_2^2-\gamma^2+4\Delta^2(t)+8J_1(t)J_2\cos(k)+4i\gamma J_2\sin(k)}}{[2J_1(t)+\gamma+2J_2e^{-ik}][\sqrt{4J_1^2(t)-\gamma^2}+2e^{ik}J_2]}, \quad \text{(A5)}$$

$$d_1=\sqrt{4J_1^2(t)+4J_2^2-\gamma^2+4\Delta^2(t)+4J_2\cos(k)\sqrt{4J_1^2(t)-\gamma^2}}. \quad \text{(A6)}$$

The factor $\alpha(k)$ in Eq. (A2) reads

$$\alpha(k)=\frac{\sqrt{4J_1^2(t)+4J_2^2-\gamma^2+4\Delta^2(t)+4J_2\cos(k)\sqrt{4J_1^2(t)-\gamma^2}}}{\sqrt{4J_1^2(t)+4J_2^2-\gamma^2+4\Delta^2(t)+8J_1(t)J_2\cos(k)+4i\gamma J_2\sin(k)}}. \quad \text{(A7)}$$

After the similaritylike transformation, the RM model is recast as a Hermitian form,

$$\hat{\mathcal{H}}(k,t)=\begin{pmatrix}\Delta(t) & \sqrt{J_1^2(t)-\frac{\gamma^2}{4}}+J_2e^{-ik}\\ \sqrt{J_1^2(t)-\frac{\gamma^2}{4}}+J_2e^{ik} & -\Delta(t)\end{pmatrix}, \quad \text{(A8)}$$

which is Eq. (6) in the main text.

APPENDIX B: EXCEPTIONAL POINTS OF RICE-MELE MODEL

It is well known that in the Hermitian Rice-Mele model, one key difference between the spectra under OBCs and PBCs is the presence of edge states in the OBC case. When the Chern number is nonzero, edge states appear under open boundary conditions (OBCs), illustrating the bulk-edge correspondence. But when non-Hermiticity is introduced (i.e., $\gamma\neq 0$), the situation changes significantly. First, we show the spectrum of the RM model under OBCs with directional intracell hopping strength, as written in Eq. (1) of the main text, and demonstrate the exceptional points. The matrix form of the RM model under OBCs is written as

$$\hat{H}(t)=\begin{pmatrix} \Delta(t) & J_1(t)+\gamma/2 & & & \cdots & & 0\\ J_1(t)-\gamma/2 & -\Delta(t) & J_2 & & & & \\ & J_2 & \Delta(t) & J_1(t)+\gamma/2 & & & \\ \vdots & & J_1(t)-\gamma/2 & -\Delta(t) & & & \vdots\\ & & & & \ddots & & \\ & & & & & \Delta(t) & J_1(t)+\gamma/2\\ 0 & & \cdots & & & J_1(t)-\gamma/2 & -\Delta(t) \end{pmatrix}. \tag{B1}$$

For this model, an exceptional point (EP) arises when $J_1(t)=J_0+E_0\cos(\omega t)=\pm\gamma/2$. Here, we take $\gamma=0.4E_0$ as an example to demonstrate the EPs in RM model. The energy spectrum when $J_0=0.5E_0<E_0+\gamma/2$ is shown in Figs. 5(a) and 5(c). It is clear that in one cycle, the system experiences EPs four times. At EPs, the energy spectrum becomes complex and the real part of the energy spectrum is coalesced. The exceptional points vanish when $J_0>E_0+\gamma/2$, as depicted in Figs. 5(b) and 5(d). In this situation, the system no longer encounters exceptional points in one pump cycle. As such, the Thouless charge pumping is well behaved.

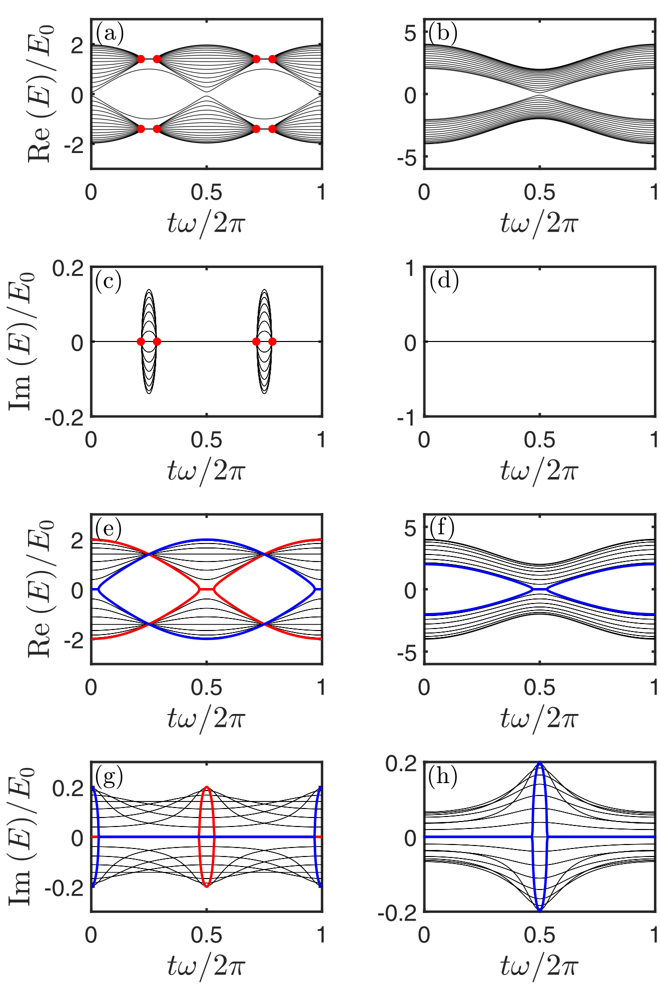

FIG. 5. Spectra of the non-Hermitian Rice-Mele model with $\gamma=0.4E_0$. (a), (c) The real and imaginary parts of energy spectra under OBC when $J_0=0E_0$. The red dots mark the location of the EPs. (b), (d) The real and imaginary parts of energy spectra under OBC when $J_0=2.02E_0$. (e), (g) The real and imaginary parts of energy spectra under PBC when $J_0=0E_0$. (f), (h) The real and imaginary parts of energy spectra under PBC when $J_0=2.02E_0$. The red line in (e) and (g) means the energy with momentum $k=0$, and the blue line in (e)–(h) means the energy with momentum $k=\pi$.

Under PBCs, most of the energy eigenvalues are complex, except for two states with momentum $k=0$ and $k=\pi$, corresponding respectively to the red line and the blue line in Figs. 5(e)–5(h). The energies of these two states become complex only when $J_0\in[-E_0+J_2-\gamma/2,-E_0+J_2+\gamma/2]$ and $J_0\in[E_0+J_2-\gamma/2,E_0+J_2+\gamma/2]$. In other words, each of these two states experiences two EPs. Therefore, both spectra under PBCs and OBCs experience EPs when J_0 varies. We return to the Chern number, which is defined from the bulk Hamiltonian. Our results show that the Chern number is ill defined (i.e., nonquantized) when $J_0\in[-E_0+J_2-\gamma/2,-E_0+J_2+\gamma/2]$ and $J_0\in[E_0+J_2-\gamma/2,E_0+J_2+\gamma/2]$. Outside these intervals, $\mathcal{PT}$ symmetry revives, and the quantized Chern number becomes well defined, as illustrated in Figs. 2(a) and 7.

APPENDIX C: WANNIER STATE AND CHARGE PUMPING UNDER RIGHT-RIGHT BASIS

After the similarity transformation [74], the charge pumping displacement $x_{\mathrm{LR}}(t)$ defined in Eq. (12) of the main text is the position expectation value under $S^{-1}(0)|w_j\rangle_{\mathrm{R}}$ and ${}_{\mathrm{L}}\langle w_j|S(0)$, which are driven by the real-space

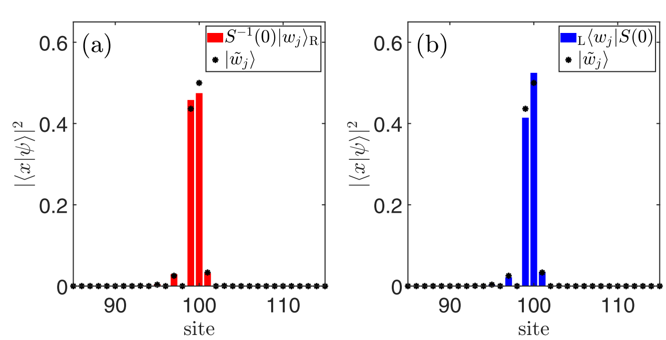

FIG. 6. The wave packet of the initial Wannier state with $\gamma=0.1E_0$ and $J_0=E_0$. (a) The red histogram depicts the right Wannier state after similarity transformation. (b) The blue histogram depicts the left Wannier state after similarity transformation. The black dots represent the initial Wannier state of the Hermitian Hamiltonian.

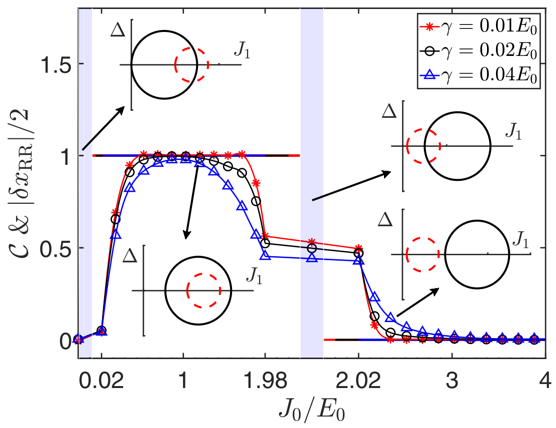

FIG. 7. The Chern number (lines) and the displacement (symbols) in a cycle under right-right vectors as a function of J_0; $\omega = 0.1E_0$. The insets are the schematics of the evolutionary path, where the red dashed line is the gapless line of the spectrum.

Hermitian Hamiltonian. In Fig. 6, the initial wave packets of $S^{-1}(0)\,|w_j\rangle_{\rm R}$ and ${}_{\rm L}\langle w_j|S(0)$ are illustrated by the red and blue histograms, respectively. The initial Wannier state of Hermitian Hamiltonian $|\tilde{w}_j\rangle$ is represented by the black dots. Those initial states are all localized in the lower band. By numerical comparison, we find that the wave packets of $S^{-1}(0)\,|w_j\rangle_{\rm R}$ [or ${}_{\rm L}\langle w_j|S(0)$] and $|\tilde{w}_j\rangle$ are approximately identical in spatial distribution, which justifies the conclusion that $|\tilde{w}_j\rangle \approx S^{-1}|w_j(m)\rangle_{\rm R}$ in the main text.

To study the topological charge pumping under the right-right basis, we show the displacement and Chern number with different γ by solid lines and symbols in Fig. 7. In contrast to the biorthogonal basis, a physical Chern number does not exist in the intervals $J_0 \in [-E_0 + J_2 - \gamma/2, -E_0 + J_2 + \gamma/2]$ and $J_0 \in [E_0 + J_2 - \gamma/2, E_0 + J_2 + \gamma/2]$, indicated by the blue interval. This is because the evolution path crosses the gapless line of the spectrum, as illustrated by the insets of Fig. 7. As γ increases, the range of the quantized topological charge pumping becomes narrower, which is consistent with the fact that the region of the quantized Chern number becomes narrower as well.

In the insets of Fig. 7, the evolutionary path and the gapless line of the spectrum are illustrated by the black solid line and the red dashed line. When the closed evolutionary path contains the entire gapless range, the Chern number is equal to 1. The gapless range of the RM model can be simply obtained from the Hamiltonian $\hat{H}(k)$. The eigenenergy of the Hamiltonian is $E_\pm = \pm\sqrt{d_x^2 + (d_y + i\gamma/2)^2 + d_z^2}$. When $E_\pm = 0$, the energy band is closed, and we find the gapless condition is $J_1(t) = \pm J_2 \pm \sqrt{\gamma^2/4 - \Delta^2(t)}$.

[1] Y. E. Kraus, Y. Lahini, Z. Ringel, M. Verbin, and O. Zilberberg, Topological states and adiabatic pumping in quasicrystals, Phys. Rev. Lett. **109**, 106402 (2012).

[2] M. Atala, M. Aidelsburger, J. T. Barreiro, D. Abanin, T. Kitagawa, E. Demler, and I. Bloch, Direct measurement of the Zak phase in topological Bloch bands, Nat. Phys. **9**, 795 (2013).

[3] G. Jotzu, M. Messer, R. Desbuquois, M. Lebrat, T. Uehlinger, D. Greif, and T. Esslinger, Experimental realization of the topological Haldane model with ultracold fermions, Nature (London) **515**, 237 (2014).

[4] Y.-K. Sun, X.-L. Zhang, F. Yu, Z.-N. Tian, Q.-D. Chen, and H.-B. Sun, Non-Abelian Thouless pumping in photonic waveguides, Nat. Phys. **18**, 1080 (2022).

[5] V. Brosco, L. Pilozzi, R. Fazio, and C. Conti, Non-Abelian Thouless pumping in a photonic lattice, Phys. Rev. A **103**, 063518 (2021).

[6] W. A. Benalcazar, J. Noh, M. Wang, S. Huang, K. P. Chen, and M. C. Rechtsman, Higher-order topological pumping and its observation in photonic lattices, Phys. Rev. B **105**, 195129 (2022).

[7] K. v. Klitzing, G. Dorda, and M. Pepper, New method for high-accuracy determination of the fine-structure constant based on quantized Hall resistance, Phys. Rev. Lett. **45**, 494 (1980).

[8] S. Raghu and F. D. M. Haldane, Analogs of quantum-Hall-effect edge states in photonic crystals, Phys. Rev. A **78**, 033834 (2008).

[9] F. D. M. Haldane and S. Raghu, Possible realization of directional optical waveguides in photonic crystals with broken time-reversal symmetry, Phys. Rev. Lett. **100**, 013904 (2008).

[10] D. J. Thouless, Quantization of particle transport, Phys. Rev. B **27**, 6083 (1983).

[11] Q. Niu and D. J. Thouless, Quantised adiabatic charge transport in the presence of substrate disorder and many-body interaction, J. Phys. A: Math. Gen. **17**, 2453 (1984).

[12] D. J. Thouless, M. Kohmoto, M. P. Nightingale, and M. den Nijs, Quantized Hall conductance in a two-dimensional periodic potential, Phys. Rev. Lett. **49**, 405 (1982).

[13] B. Simon, Holonomy, the quantum adiabatic theorem, and Berry's phase, Phys. Rev. Lett. **51**, 2167 (1983).

[14] L. Privitera, A. Russomanno, R. Citro, and G. E. Santoro, Nonadiabatic breaking of topological pumping, Phys. Rev. Lett. **120**, 106601 (2018).

[15] M. Jürgensen, S. Mukherjee, and M. C. Rechtsman, Quantized nonlinear Thouless pumping, Nature (London) **596**, 63 (2021).

[16] S. Nakajima, T. Tomita, S. Taie, T. Ichinose, H. Ozawa, L. Wang, M. Troyer, and Y. Takahashi, Topological Thouless pumping of ultracold fermions, Nat. Phys. **12**, 296 (2016).

[17] P. B. Ndiaye, C. A. Akosa, M. H. Fischer, A. Vaezi, E.-A. Kim, and A. Manchon, Dirac spin-orbit torques and charge pumping at the surface of topological insulators, Phys. Rev. B **96**, 014408 (2017).

[18] P. Marra, R. Citro, and C. Ortix, Fractional quantization of the topological charge pumping in a one-dimensional superlattice, Phys. Rev. B **91**, 125411 (2015).

[19] F. Yang, X. Li, and H. Zhai, Nonadiabatic effect in topological and interacting charge pumping, Phys. Rev. B **109**, 064301 (2024).

[20] S. Greschner, S. Mondal, and T. Mishra, Topological charge pumping of bound bosonic pairs, Phys. Rev. A **101**, 053630 (2020).

[21] Z. Sun and A. J. Millis, Topological charge pumping in excitonic insulators, Phys. Rev. Lett. **126**, 027601 (2021).

[22] L. Wang, M. Troyer, and X. Dai, Topological charge pumping in a one-dimensional optical lattice, Phys. Rev. Lett. **111**, 026802 (2013).

[23] M. M. Wauters, A. Russomanno, R. Citro, G. E. Santoro, and L. Privitera, Localization, topology, and quantized transport in disordered Floquet systems, Phys. Rev. Lett. **123**, 266601 (2019).

[24] M. Jürgensen and M. C. Rechtsman, Chern number governs soliton motion in nonlinear Thouless pumps, Phys. Rev. Lett. **128**, 113901 (2022).

[25] K. Takahashi, K. Fujii, Y. Hino, and H. Hayakawa, Nonadiabatic control of geometric pumping, Phys. Rev. Lett. **124**, 150602 (2020).

[26] S. Nakajima, N. Takei, K. Sakuma, Y. Kuno, P. Marra, and Y. Takahashi, Competition and interplay between topology and quasi-periodic disorder in Thouless pumping of ultracold atoms, Nat. Phys. **17**, 844 (2021).

[27] M. Lohse, C. Schweizer, O. Zilberberg, M. Aidelsburger, and I. Bloch, A Thouless quantum pump with ultracold bosonic atoms in an optical superlattice, Nat. Phys. **12**, 350 (2016).

[28] D. Dreon, A. Baumgärtner, X. Li, S. Hertlein, T. Esslinger, and T. Donner, Self-oscillating pump in a topological dissipative atom–cavity system, Nature (London) **608**, 494 (2022).

[29] O. Zilberberg, S. Huang, J. Guglielmon, M. Wang, K. P. Chen, Y. E. Kraus, and M. C. Rechtsman, Photonic topological boundary pumping as a probe of 4D quantum Hall physics, Nature (London) **553**, 59 (2018).

[30] A. Cerjan, M. Wang, S. Huang, K. P. Chen, and M. C. Rechtsman, Thouless pumping in disordered photonic systems, Light: Sci. Appl. **9**, 178 (2020).

[31] W. Liu, C. Wu, Y. Jia, S. Jia, G. Chen, and F. Chen, Observation of edge-to-edge topological transport in a photonic lattice, Phys. Rev. A **105**, L061502 (2022).

[32] J. Luneau, C. Dutreix, Q. Ficheux, P. Delplace, B. Douçot, B. Huard, and D. Carpentier, Topological power pumping in quantum circuits, Phys. Rev. Res. **4**, 013169 (2022).

[33] S. Malzard, C. Poli, and H. Schomerus, Topologically protected defect states in open photonic systems with non-Hermitian charge-conjugation and parity-time symmetry, Phys. Rev. Lett. **115**, 200402 (2015).

[34] Y. Choi, S. Kang, S. Lim, W. Kim, J.-R. Kim, J.-H. Lee, and K. An, Quasieigenstate coalescence in an atom-cavity quantum composite, Phys. Rev. Lett. **104**, 153601 (2010).

[35] T. E. Lee, F. Reiter, and N. Moiseyev, Entanglement and spin squeezing in non-Hermitian phase transitions, Phys. Rev. Lett. **113**, 250401 (2014).

[36] Y. Ashida, Z. Gong, and M. Ueda, Non-Hermitian physics, Adv. Phys. **69**, 249 (2020).

[37] K. Kawabata, T. Numasawa, and S. Ryu, Entanglement phase transition induced by the non-Hermitian skin effect, Phys. Rev. X **13**, 021007 (2023).

[38] B. Gardas, S. Deffner, and A. Saxena, Non-Hermitian quantum thermodynamics, Sci. Rep. **6**, 23408 (2016).

[39] K. Kawabata, S. Higashikawa, Z. Gong, Y. Ashida, and M. Ueda, Topological unification of time-reversal and particle-hole symmetries in non-Hermitian physics, Nat. Commun. **10**, 297 (2019).

[40] J. Li, A. K. Harter, J. Liu, L. de Melo, Y. N. Joglekar, and L. Luo, Observation of parity-time symmetry breaking transitions in a dissipative Floquet system of ultracold atoms, Nat. Commun. **10**, 855 (2019).

[41] Z. Ren, D. Liu, E. Zhao, C. He, K. K. Pak, J. Li, and G.-B. Jo, Chiral control of quantum states in non-Hermitian spin–orbit-coupled fermions, Nat. Phys. **18**, 385 (2022).

[42] Q. Liang, D. Xie, Z. Dong, H. Li, H. Li, B. Gadway, W. Yi, and B. Yan, Dynamic signatures of non-Hermitian skin effect and topology in ultracold atoms, Phys. Rev. Lett. **129**, 070401 (2022).

[43] K. Sun and W. Yi, Chiral state transfer under dephasing, Phys. Rev. A **108**, 013302 (2023).

[44] W. Chen, M. Abbasi, Y. N. Joglekar, and K. W. Murch, Quantum jumps in the non-Hermitian dynamics of a superconducting qubit, Phys. Rev. Lett. **127**, 140504 (2021).

[45] W. Chen, M. Abbasi, B. Ha, S. Erdamar, Y. N. Joglekar, and K. W. Murch, Decoherence-induced exceptional points in a dissipative superconducting qubit, Phys. Rev. Lett. **128**, 110402 (2022).

[46] L. Xiao, X. Zhan, Z. Bian, K. Wang, X. Zhang, X. Wang, J. Li, K. Mochizuki, D. Kim, N. Kawakami *et al.*, Observation of topological edge states in parity–time-symmetric quantum walks, Nat. Phys. **13**, 1117 (2017).

[47] W.-C. Wang, Y.-L. Zhou, H.-L. Zhang, J. Zhang, M.-C. Zhang, Y. Xie, C.-W. Wu, T. Chen, B.-Q. Ou, W. Wu, H. Jing, and P.-X. Chen, Observation of $\mathcal{PT}$-symmetric quantum coherence in a single-ion system, Phys. Rev. A **103**, L020201 (2021).

[48] L. Ding, K. Shi, Q. Zhang, D. Shen, X. Zhang, and W. Zhang, Experimental determination of $\mathcal{PT}$-symmetric exceptional points in a single trapped ion, Phys. Rev. Lett. **126**, 083604 (2021).

[49] Z. Gong, Y. Ashida, K. Kawabata, K. Takasan, S. Higashikawa, and M. Ueda, Topological phases of non-Hermitian systems, Phys. Rev. X **8**, 031079 (2018).

[50] E. Edvardsson, F. K. Kunst, and E. J. Bergholtz, Non-Hermitian extensions of higher-order topological phases and their biorthogonal bulk-boundary correspondence, Phys. Rev. B **99**, 081302(R) (2019).

[51] S. Longhi, Unraveling the non-Hermitian skin effect in dissipative systems, Phys. Rev. B **102**, 201103(R) (2020).

[52] L. Pan, X. Chen, Y. Chen, and H. Zhai, Non-Hermitian linear response theory, Nat. Phys. **16**, 767 (2020).

[53] J. Li, T. Prosen, and A. Chan, Spectral statistics of non-Hermitian matrices and dissipative quantum chaos, Phys. Rev. Lett. **127**, 170602 (2021).

[54] X. Zhan, L. Xiao, Z. Bian, K. Wang, X. Qiu, B. C. Sanders, W. Yi, and P. Xue, Detecting topological invariants in nonunitary discrete-time quantum walks, Phys. Rev. Lett. **119**, 130501 (2017).

[55] D. Hao, L. Wang, X. Lu, X. Cao, S. Jia, Y. Hu, and Y. Xiao, Topological atomic spin wave lattices by dissipative couplings, Phys. Rev. Lett. **130**, 153602 (2023).

[56] K. Kawabata, K. Shiozaki, M. Ueda, and M. Sato, Symmetry and topology in non-Hermitian physics, Phys. Rev. X **9**, 041015 (2019).

[57] E. J. Bergholtz, J. C. Budich, and F. K. Kunst, Exceptional topology of non-Hermitian systems, Rev. Mod. Phys. **93**, 015005 (2021).

[58] C. Poli, M. Bellec, U. Kuhl, F. Mortessagne, and H. Schomerus, Selective enhancement of topologically induced interface states in a dielectric resonator chain, Nat. Commun. **6**, 6710 (2015).

[59] M.-A. Miri and A. Alu, Exceptional points in optics and photonics, Science **363**, eaar7709 (2019).

[60] Ş. K. Özdemir, S. Rotter, F. Nori, and L. Yang, Parity–time symmetry and exceptional points in photonics, Nat. Mater. **18**, 783 (2019).

[61] Z. Feng and X. Sun, Harnessing dynamical encircling of an exceptional point in anti-$\mathcal{PT}$-symmetric integrated photonic systems, Phys. Rev. Lett. **129**, 273601 (2022).

[62] X. Shu, A. Li, G. Hu, J. Wang, A. Alù, and L. Chen, Fast encirclement of an exceptional point for highly efficient and compact chiral mode converters, Nat. Commun. **13**, 2123 (2022).

[63] S. Longhi, Probing non-Hermitian skin effect and non-Bloch phase transitions, Phys. Rev. Res. **1**, 023013 (2019).

[64] A. Kumar, S. Mazumdar, S. Mahanti, and K. Saha, Anomalous pumping in the non-Hermitian Rice-Mele model, J. Phys.: Condens. Matter **37**, 135601 (2025).

[65] Z. Zhang, T. Li, X.-W. Luo, and W. Yi, Biorthogonal topological charge pumping in non-Hermitian systems, Phys. Rev. B **109**, 224307 (2024).

[66] M. Ezawa, N. Ishida, Y. Ota, and S. Iwamoto, Nonadiabatic nonlinear non-Hermitian quantized pumping, Phys. Rev. Res. **6**, 033258 (2024).

[67] K. Kyriakou and K. Moulopoulos, Emergent non-Hermitian boundary contributions to charge pumping and electric polarization, arXiv:2106.14173.

[68] Z. Fedorova, H. Qiu, S. Linden, and J. Kroha, Observation of topological transport quantization by dissipation in fast Thouless pumps, Nat. Commun. **11**, 3758 (2020).

[69] C. Yuce, Spontaneous topological pumping in non-Hermitian systems, Phys. Rev. A **99**, 032109 (2019).

[70] B. Höckendorf, A. Alvermann, and H. Fehske, Topological origin of quantized transport in non-Hermitian Floquet chains, Phys. Rev. Res. **2**, 023235 (2020).

[71] L. Li, C. H. Lee, and J. Gong, Topology-induced spontaneous non-reciprocal pumping in cold-atom systems with loss, Phys. Rev. Lett. **124**, 250402 (2020).

[72] M. J. Rice and E. J. Mele, Elementary excitations of a linearly conjugated diatomic polymer, Phys. Rev. Lett. **49**, 1455 (1982).

[73] J. K. Asbóth, L. Oroszlány, and A. Pályi, *A Short Course on Topological Insulators* (Springer, Heidelberg, 2016), p. 46.

[74] S. Yao and Z. Wang, Edge states and topological invariants of non-Hermitian systems, Phys. Rev. Lett. **121**, 086803 (2018).

[75] S. Yao, F. Song, and Z. Wang, Non-Hermitian Chern bands, Phys. Rev. Lett. **121**, 136802 (2018).

[76] L. Xiao, T. Deng, K. Wang, G. Zhu, Z. Wang, W. Yi, and P. Xue, Non-Hermitian bulk–boundary correspondence in quantum dynamics, Nat. Phys. **16**, 761 (2020).

[77] K. Wang, T. Li, L. Xiao, Y. Han, W. Yi, and P. Xue, Detecting non-Bloch topological invariants in quantum dynamics, Phys. Rev. Lett. **127**, 270602 (2021).

[78] P. Wang, Z.-Q. Yu, Z. Fu, J. Miao, L. Huang, S. Chai, H. Zhai, and J. Zhang, Spin-orbit coupled degenerate Fermi gases, Phys. Rev. Lett. **109**, 095301 (2012).

[79] M. Mancini, G. Pagano, G. Cappellini, L. Livi, M. Rider, J. Catani, C. Sias, P. Zoller, M. Inguscio, M. Dalmonte, and L. Fallani, Observation of chiral edge states with neutral fermions in synthetic Hall ribbons, Science **349**, 1510 (2015).